ResearchGate

See discussions, stats, and author profiles for this publication at: https://www.researchgate.net/publication/229860418

Kinetic Studies of the Reactions of IO Radicals Determined by Cavity Ring-Down Spectroscopy

ARTICLE *in* THE JOURNAL OF PHYSICAL CHEMISTRY A · AUGUST 1999

Impact Factor: 2.69 · DOI: 10.1021/jp9902497

CITATIONS
41

READS
22

3 AUTHORS, INCLUDING:

Jeffrey W Hudgens
National Institute of Standards and Technolo…

135 PUBLICATIONS **2,208** CITATIONS

SEE PROFILE

Available from: Jeffrey W Hudgens
Retrieved on: 16 January 2016

Kinetic Studies of the Reactions of IO Radicals Determined by Cavity Ring-Down Spectroscopy

Dean B. Atkinson[†] **and Jeffrey W. Hudgens***

Physical and Chemical Properties Division, National Institute of Standards and Technology, Gaithersburg, Maryland 20899

Andrew J. Orr-Ewing

School of Chemistry, University of Bristol, Cantock's Close, Bristol BS8 1TS, U.K.

Received: January 21, 1999

We demonstrate the application of cavity ring-down spectroscopy (CRDS) to the measurement of concentrations of IO radical and of reaction rate coefficients for the reaction systems, IO + IO and IO + NO, using the source reaction, $O(^3P) + CF_3I$. By monitoring IO radicals, we obtain the 295 K rate coefficients, $k(O + CF_3I \rightarrow IO + CF_3) = (5.8 \pm 1.5) \times 10^{-12}$ cm^3 molec^{-1} s^{-1}; $k(IO + IO) = (1.0 \pm 0.3) \times 10^{-10}$ cm^3 molec^{-1} s^{-1}, and $k(IO + NO) = (1.9 \pm 0.5) \times 10^{-11}$ cm^3 molec^{-1} s^{-1} at the pressures of 1250 Pa (9.4 Torr) and 4000 Pa (30.1 Torr). For the IO A $^2\Pi_{3/2} - X\ ^2\Pi_{3/2}$ (2, 0) bandhead at 445.04 nm we have determined an absorption cross-section, $\sigma = (7.3 \pm 0.7) \times 10^{-17}$ cm^2. Error limits indicate the confidence of two standard deviations and propagate the uncertainty in the absorption cross-section.

1. Introduction

Sensitive, precise, and quantitative methods for studying the reactions of IO are necessary to clarify the role of this radical in the chemistry of earth's troposphere and stratosphere.[1] Atmospheric iodine compounds are principally biogenic in origin, and CH_3I from marine algal emissions is rapidly photolyzed in the troposphere, liberating iodine which may react with ozone to form IO. The subsequent reactions of IO can influence tropospheric ozone concentrations,[2] and elevated IO concentrations are suspected to arise in the lower troposphere over the Arctic in the springtime, coinciding with reduced ozone episodes.[3,4] Rapid convective transport of CH_3I to the upper troposphere and lower stratosphere has been postulated[3] and would result in formation of IO at altitudes where it may participate in catalytic stratospheric ozone destruction cycles. The possible existence of these processes is evidenced by the recent detection of the IO radical in the marine boundary layer.[5]

Several studies have been performed of the kinetics of reactions of IO using laser photolysis and detection of IO via absorption spectroscopy[6−9] or laser induced fluorescence (LIF).[10−15] Such methods have established values of rate coefficients for the IO + IO self-reaction,[7−9] and for reaction of IO with NO,[13,15,16] Br,[11] BrO,[7,12] ClO,[14] $CHCl_2CF_2Cl$,[17] HCOOH,[17] and dimethyl sulfide,[18] to name a few. The current study, however, is the first use of cavity ring-down spectroscopy (CRDS)[19−21] for detection of IO and determination of its reaction rates, and demonstrates the suitability of combining CRDS with laser photolysis methods for accurate kinetics studies of species such as IO. Since the introduction of CRDS detection to the field of kinetics by M. C. Lin,[22,23] CRDS detection has become increasingly used for rate coefficient determinations. To date, CRDS has been used to study reactions of the phenyl,[22−26] NH_2,[27] and propargyl radicals,[28] the kinetics of the C_2H_5/$C_2H_5O_2$[29] and vinoxy/O_2 systems,[30] and the chlorine and bromine adducts of propargyl halides[31] and allene.[32] Where comparisons have been made with well-established rate coefficients determined by methods other than CRDS, the agreement has been excellent,[29] but validation of the CRDS method for kinetics studies has not been extensively investigated. The current study provides a direct comparison of reaction rate coefficients measured both for detection of IO via a sharply structured, rotationally resolved spectrum and via a diffuse, unstructured absorption spectrum. The results show quantitative agreement with the previous LIF and absorption spectroscopy studies. We concentrate on the reactions of IO + IO and IO + NO because these have been the subject of several previous studies, thereby allowing a careful comparison of our CRDS-based results with other experimental methods, and because of their importance in linking the atmospheric chemistry of iodine with that of NO_x species and in determining the partitioning of atmospheric iodine between I and IO. The use of CRDS detection to determine rates of reaction of IO suggests a sensitive method for studying the reactions of the BrO radical. BrO exhibits no A $^2\Pi - X\ ^2\Pi$ LIF spectrum because of rapid predissociation of the A $^2\Pi$ state, but the effectiveness of CRDS detection of this radical has already been demonstrated.[33]

2. Experimental

The laser photolysis/cavity ring-down kinetic apparatus used to measure the rates of reactions of IO has been described in detail elsewhere[28,29] and will only be summarized briefly here. Experiments were conducted in a quartz flow tube with high reflectivity (HR) mirrors located at either end; these mirrors define the ring-down cavity (RDC). The HR mirrors were held in adjustable mounts attached to the flow tube via flexible bellows and positioned 1.1 m apart. Reaction was initiated by

* Author for correspondence. E-mail: jeffrey.hudgens@nist.gov. Fax: 301-975-3672.

[†] Current address: Chemistry Department, Portland State University, Portland, OR 97207-0751.

10.1021/jp9902497 CCC: $18.00 © 1999 American Chemical Society
Published on Web 07/14/1999

laser photolysis and reaction products were probed at a variable delay after initiation by cavity ring-down absorption detection using a second laser pulse. The extent of absorption was determined by monitoring the ring-down decay rate of the laser pulse within the cavity, and typical 1/e decay times for the ring-down were 1 μs. The variation of IO absorption with time delay between pulses can be analyzed (assuming Beer−Lambert absorption behavior) to give the desired reaction rates. During these experiments the ambient temperature of the laboratory and reactor was 295 K.

IO was produced in the RDC by 193 nm photolysis of N_2O in the presence of CF_3I (>97% and used without further purification) and argon buffer gas. Flows of these gases into the RDC were regulated by mass flow controllers. An ArF excimer laser was used to produce ca. maximum energy = 100 mJ, 20 ns duration pulses of 193 nm UV at 5 Hz repetition rate which after beam steering and shaping placed a flux of $\leq$ 6 mJ cm^{-2} into the photolysis zone of the reactor. The laser pulses were shaped into 6-cm long, 1-cm high stripes by a cylindrical lens and a beam mask and intersected the RDC perpendicular to the axis defined by the HR mirrors. UV photolysis of N_2O generated $O(^1D)$ which underwent rapid collisional quenching to form $O(^3P)$. Contamination of the mirrors over the duration of the experiment was minimized by flushing argon gas through separately pumped regions of the RDC immediately in front of the mirrors. The flow of Ar through these regions was regulated so that the pressure matched the total pressure in the central region of the RDC, as has been described in detail previously. For reactions involving NO, the NO (either neat or ca. 5% in Ar) was passed through a copper coil immersed in a dry ice/acetone slush bath to remove contaminant NO_2 and was introduced into the RDC via a mass flow controller.

A pulsed dye laser pumped by the output of a XeCl excimer laser produced the probe laser light at wavelengths in the range between 445 and 470 nm. The dye laser operated on coumarin 440 dye, and the output energy was typically between 1 and 5 mJ per pulse at 5 Hz repetition rate. The probe laser was injected into the RDC through one end mirror. For a beam waist of 0.32 mm and a mirror reflectivity of R $\approx$ 99.9%, the maximum cavity flux is $\leq$5 mJ cm^{-2}. The mirror alignment was carefully adjusted to give an exponential decay of the light intensity within the cavity, with maximum suppression of interference effects caused by beating between transverse cavity modes as described in detail elsewhere.[29] Light exiting the other end mirror was imaged through a pinhole onto a quartz diffuser and photomultiplier tube. For kinetics experiments the laser wavelength corresponded either to excitation of IO on the bandhead of the highly structured IO A−X (2, 0) band at λ_{CRDS} = 445.04 nm or at the bandhead of the much weaker and diffuse IO A−X (1, 0) band at λ_{CRDS} = 455.17 nm.

For each laser shot, the exponential decay of the laser light intensity within the cavity, as detected by the photomultiplier, was digitized using a digital oscilloscope and transferred to a personal computer via an IEEE-488 interface for analysis. Each decay trace was fitted separately to a first-order exponential decay, and the resultant ring-down rates were averaged for each time delay between the two lasers. Ring-down decay rates were converted to absorbances via standard relationships.[29] The time delay between photolysis and probe lasers was selected randomly within a predetermined range by a programmed pulse delay generator, and 10 laser shots were averaged at that delay time to produce one data point. Typically, data points at 100 different delay settings were accumulated to define each IO temporal decay trace, with the effects of small drifts in the experimental conditions reduced by the random, rather than systematic, variation of the delay times. We measured the base system absorbance immediately before each kinetic absorbance measurement at a given reaction time. This zeroing procedure eliminated system drift and confined the measurement of absorbance change to the 6-cm long photolysis zone.

The kinetic experiments produce transient absorption (which is readily converted to radical concentration) vs time. To derive rate coefficients from these data, the kinetic mechanism is designed and the absorption data is computationally simulated. This simulation is compared to the observed data and the χ^2 value is computed. Using the Levenberg−Marquardt procedure,[34] selected rate coefficients and concentrations are varied to minimize this value. The simulation software comprises of a custom graphic interface that spawns satellite shells executing the original FORTRAN code of the ACUCHEM program[35] that simulates kinetics through numerical forward integration of a reaction mechanism. The accuracy of this program has been verified.[35]

3. Results and Analyses

The 193 nm photolysis of N_2O in the mixture of N_2O, CF_3I, NO, and argon results in the formation and loss of IO and NO via the following kinetic scheme:

$$N_2O + h\nu\ (\lambda = 193\ nm) \rightarrow N_2 + O(^1D) \quad (1)$$

$$O(^1D) + M \rightarrow O(^3P) + M\ (M = Ar, N_2O, CF_3I, NO) \quad (2)$$

$$O(^1D) + N_2O \rightarrow NO + NO \quad (3a)$$

$$\rightarrow N_2 + O_2 \quad (3b)$$

$$O(^3P) + NO + Ar \rightarrow NO_2 + Ar \quad (4)$$

$$O(^3P) + CF_3I \rightarrow IO + CF_3 \quad (5a)$$

$$\rightarrow CF_2O + IF \quad (5b)$$

$$\rightarrow CF_3OI \quad (5c)$$

$$IO + IO \rightarrow I_2 + O_2 \quad (6a)$$

$$\rightarrow I + OIO \quad (6b)$$

$$\rightarrow I_2O_2 \quad (6c)$$

$$\rightarrow 2I + O_2 \quad (6d)$$

$$IO + NO \rightarrow I + NO_2 \quad (7)$$

$$IO + O(^3P) \rightarrow O_2 + I \quad (8)$$

$$IO \rightarrow products \quad (9)$$

The unimolecular process in reaction 9 corresponds to wall loss or diffusion.

Reactions 2 and 3 describe the competition between the collisional deactivation of $O(^1D)$ and its reaction with N_2O. Reactions 4 and 7 produce NO_2. We have accounted for NO_2 production because its optical absorption continuum overlaps with the IO spectrum. The reaction rate coefficients of k_3 and the termolecular rate coefficient k_4 are known[36] as are the deactivation rate coefficients of $O(^1D)$ by Ar,[37] NO,[38] and N_2O.[36] The deactivation rate coefficient of $O(^1D)$ by CF_3I is unknown; however, extrapolation of the homologous series of $k_2(CF_3Cl) = 4.2 \times 10^{-12}$ cm^3 $molec^{-1}$ s^{-1} [39] and $k_2(CF_3Br) = 5.9 \times 10^{-11}$ cm^3 $molec^{-1}s^{-1}$ [40] would predict that $k_2(CF_3I)$ is considerably

larger than $k_2(CF_3Br)$. Thus, as in previous studies,[7,8,10] the large global deactivation rate will quench the $O(^1D)$ population to $O(^3P)$ within nanoseconds and allow us to ignore the effects of any residual NO from reaction 3. This conclusion was confirmed during our modeling of the IO absorption data.

Reaction 5 has three exothermic channels. Gilles et al.[41] determined that channel 5a accounts for 83% of the products. Little consensus exists regarding the products of reaction 6. Two studies have concluded that channel 6a constitutes less than 5% of the total reaction.[7,42] The observation of a spectrum of OIO suggests that channel 6b may be active; however, the mechanism for OIO production was not established.[43] To fit data for the reaction of IO + BrO, Laszlo et al.[6] postulated that between 30 and 40% of the products followed channel 6c. Harwood et al.[8] also concluded that channel 6c is important and that the sum of channels 6b and 6d accounts for as much as 50% of the reactivity.

Kinetic traces of the rise and fall of the IO signal were obtained over intervals corresponding to the delay between photolysis and probe lasers of up to 50 ms. Because a numerical model of diffusion between the CRD axis and the reactor walls predicted that wall loss (reaction 9) may begin to affect the CRD signal for times exceeding 20 ms, we did not use data observed beyond this time for derivation of reaction rate coefficients.

Although data beyond 20 ms were not used to derive rate coefficients, we obtained such data and examined it as part of our larger effort to ensure that no aerosols were forming during these experiments. Previous studies of IO radical reactions have noted that these systems have a propensity to form aerosols,[7,41,42,44] and Cox et al.[44] have proposed that these aerosols are composed of I_4O_9. The presence of aerosols will corrupt determinations of rate coefficients by accelerating the loss of IO radicals. During a CRDS experiment the light scattering induced by aerosols would cause an apparent increase of absorbance, and this signature would also be evidenced during the kinetic modeling of absorption data. During all experiments we observed the decay of IO absorbance from its maximum over intervals up to 50 ms and never detected an increase in system absorbance. The absence of an optical signature evidencing aerosols showed that aerosols, if formed at all, were produced after the experimental measurement process had concluded. The absence of deposits on the reactor walls is evidence that aerosols did not form during the 200 ms interval between each experiment. Finally, even if such aerosols were formed, our experimental procedure assured that they were removed before each measurement. During a recent study of propargyl radical kinetics, a kinetic system where soot deposits occur, we were able to experimentally measure the time required for our apparatus to remove stable, volatile, photolytic reaction products from the CRDS cavity.[28] Armed with this knowledge, we adjusted our reactor flow conditions and laser repetition rate to ensure that the reactor contents were completely refreshed between each laser pulse. In short, no physical or optical data evidencing aerosols or particulates were ever observed under the experimental conditions of the present study.

3.1. IO CRD Spectra and Absorption Cross-Sections. CRD spectra of the IO $A^2\Pi_{3/2} - X^2\Pi_{3/2}$ (2, 0), (1, 0), and (0, 0) bands were recorded with typical gas flows of 60 standard cubic centimeters per minute (sccm) of N_2O, 3 sccm of CF_3I, and 1000 sccm of Ar, with the pump throttled to give a total pressure of 4000 Pa (30.1 Torr). As an example of the sensitivity of CRDS detection, Figure 1 shows representative spectra of the IO (1, 0) and IO (2, 0) bands from the A $^2\Pi_{3/2}$ − X $^2\Pi_{3/2}$ transition. These spectra were obtained when the delay between

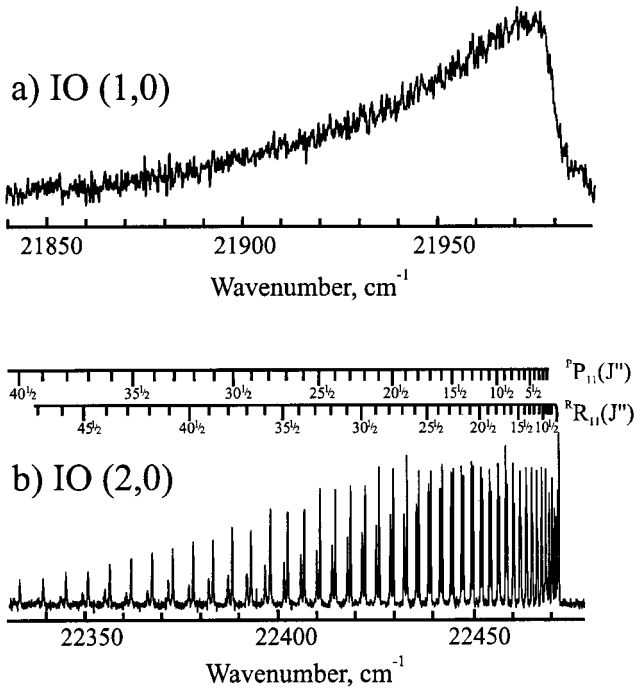

Figure 1. CRD spectra of (a) the IO A $^2\Pi_{3/2}$ − X $^2\Pi_{3/2}$ (1, 0) band and (b) part of the IO A $^2\Pi_{3/2}$ − X $^2\Pi_{3/2}$ (2, 0) band. Combs above the spectrum indicate the rotational line assignments. The relative vertical axes differ between Figure 1a and 1b. See text.

the photolysis and CRD laser pulses was 500 μs. The IO (1, 0) band is weak and diffuse, showing no discernible rotational structure, and is not observed by LIF because of rapid predissociation of IO A $^2\Pi_{3/2}$ $v = 1$. The detailed analyses of these and other IO CRD spectra and the information they contain about the predissociation of the A-state are presented elsewhere.[45]

The broad, unstructured nature of the IO (1, 0) band makes it well suited, in principle, to CRDS detection for kinetics measurements, whereas use of the sharp rotational structure of the IO (2, 0) band requires greater care. To apply CRDS detection to the accurate measurement of rate coefficients, we must ensure that all cavity modes excited by the probe laser decay at the same rate. If the absorption feature used to monitor concentrations of a radical or molecule is narrower than the laser bandwidth, the cavity modes excited by the laser and overlapped by the absorption line will decay (ring down) faster than those not spanned by the absorption. The resultant ring-down decay measured for each laser pulse will thus not be a single exponential, and ring-down rates will not be straightforwardly related to the concentration of the absorber.[46] The bandhead of the IO (2, 0) band, although discrete, is sufficiently broad to extinguish all cavity modes excited by the probe laser equally, but isolated rotational lines have Doppler and pressure-broadened widths comparable to the laser bandwidth. Kinetics measurements were thus made by tuning the probe laser either to the bandhead of the IO (2, 0) band at $\lambda_{CRDS} = 445.04$ nm or the IO (1, 0) band at $\lambda_{CRDS} = 455.17$ nm. The latter measurements will be less sensitive because of the inherent weakness of the IO (1, 0) band.

To derive rate coefficients of the second-order reaction 6, IO + IO, we need accurate absorption cross-sections, σ_λ, for the IO (1, 0) and IO (2, 0) bands. Although two previously reported, low resolution spectra ($\Delta\lambda \approx 0.8$ nm fwhm[7] and $\Delta\lambda \approx 0.44$ nm fwhm[8]) obtained with monochromators do not exhibit rotational fine structure, these spectra contain the

intensity data that enable the renormalization of the rotationally resolved CRD spectrum ($\Delta\lambda \approx 0.0013$ nm) to find σ_λ.

Absorption experiments measure an average absorption cross-section, $\sigma_\lambda^{\text{eff}}$, that is weighted by a normalized instrument function, $S(\tau)$, e.g.,

$$\sigma_\lambda^{\text{eff}} = \int_{-\Delta\lambda/2}^{\Delta\lambda/2} I(\lambda+\tau)\, S^{\text{instrument}}(\tau)\mathrm{d}\tau \qquad (10)$$

where $I(\lambda)$ is the spectrum of the molecule and $\Delta\lambda$ is the spectral width of nonzero values of $S(\tau)$. For a CRD experiment, $S^{\text{CRD}}(\tau)$ is nonzero over the width of a single cavity mode. (As mentioned above, when more than one cavity mode is active, the spectrum must observe equal σ_λs to attain good absorbance measurements.) Under the conditions that permit good CRDS measurements, $I(\lambda)$ is constant over $\Delta\lambda$ and eq 10 reduces to $\sigma_\lambda \equiv \sigma_\lambda^{\text{eff}} = I(\lambda)d\lambda^{\text{o}}$, where $d\lambda^{\text{o}}$ is the unit length. This condition occurs for the CRD spectra of the IO (2, 0) and IO (1, 0) bands.

For measurements involving a monochromator, $S^{\text{mono}}(\tau)$ is the slit function. The monochromators used in previous studies could not resolve the rotational spectrum of the IO (2, 0) band. Thus, the fine structure of $I(\lambda)$ was convoluted with $S^{\text{mono}}(\tau)$, and each observed spectrum was simply a broadened, weighted average of the rotational intensity envelope. Since the $S^{\text{mono}}(\tau)$ of each monochromator system is unique, the previously reported absorption cross-sections of the IO (2, 0) bands[7−9,44] are effective cross-sections, $\sigma_\lambda^{\text{eff}}$, that are suitable only for concentration measurements within the specific apparatus.

Using knowledge of $S^{\text{mono}}(\tau)$, we can convolute the $I(\lambda)$ observed by CRDS and compute the band profile observed by the monochromator. Since the maximum of this computed profile is proportional to $\sigma_\lambda^{\text{eff}}$, we can renormalize $I(\lambda)$ to absolute cross-section, thus, determining σ_λ for each rotational line within the IO (2, 0) band, hence enabling us to determine the concentration of IO with the CRDS spectrum. To obtain this normalization factor, we used the calibration slit function of the 0.25 m monochromator and $\sigma_\lambda^{\text{eff}} = 1.05 \times 10^{-17}$ cm^2 measured by Laszlo et al.[7] during their study of the IO spectrum. We also confirmed this $S^{\text{mono}}(\tau)$ by rescanning the monochromator over the 435.8 nm mercury emission line. This $S^{\text{mono}}(\tau)$ (0.7 nm fwhm and 1.2 nm full-width) was used in eq 10 to convolute the CRD spectrum, $I(\lambda)$. The renormalized spectrum found $\sigma_{445}^{\text{IO}} = (7.3 \pm 0.7) \times 10^{-17}$ cm^2 for the IO (2, 0) bandhead at 445.04 nm, where the uncertainty represents two standard deviations. An intuitive way to look at this renormalization process is to view the rotational spectrum as a set of boxes, each of which contains either a rotational line or no intensity at all. The ratio of $\sigma_{445}^{\text{IO}}/\sigma_\lambda^{\text{eff}} = 7$ indicates that only ~1/7 of all boxes contain a rotational line. The low resolution monochromator is averaging many resolution boxes of which 6 of every 7 contains zero absorbance.

The absorption cross-section of the IO (1, 0) band is determined from the ratio of the transient absorbance maxima of the IO (2, 0) and IO (1, 0) bands obtained from transient absorption signals observed under the same flow reactor conditions. Figure 2 shows an example of these transient signal measurements. The ratio of the transient maxima at t $\approx$ 180 μs is $A_{445}^{\text{IO(2,0)}}/A_{455}^{\text{IO(1,0)}} = 0.1 \pm 0.01$, which leads to $\sigma_{455}^{\text{IO}} = (7.3 \pm 0.7) \times 10^{-18}$ cm^2 for the cross-section of the IO (1, 0) band at 455.17 nm. For comparison, Harwood et al.[8] obtained $\sigma_{455}^{\text{IO}} = 8 \times 10^{-18}$ cm^2 and the laser absorption experiment of Stickel et al.[9] obtained $\sigma_{455}^{\text{IO}} = 6.2 \times 10^{-18}$ cm^2. The CRDS measurement may be compared directly with these prior measurements because the rotational lines of the IO (1, 0) band are homogeneously broadened into a continuum and because the resolution of both experiments ($\Delta\lambda \approx 0.44$ nm[8] and $\Delta\lambda = 0.01$ nm,[9] respectively) were of sufficient resolution to simplify eq 10 to $\sigma_\lambda = I(\lambda)d\lambda^{\text{o}}$. The accord between the CRDS and these conventional absorption measurements of σ_{455}^{IO} increases confidence in the accuracy of our derived cross-section at the bandhead of IO (2, 0), σ_{445}^{IO}.

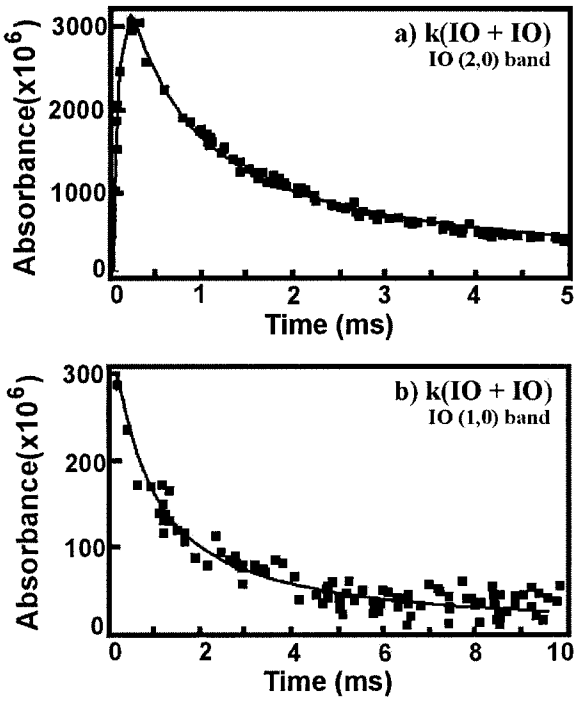

Figure 2. Kinetic measurements that determine k_6(IO + IO). Squares show absorbance as a function of the time delay between the photolysis laser pulse that initiates IO formation and the CRDS laser pulse that probes absorbance. The reagent flows of both measurements are identical and the pressure is 4015 Pa. The fits to the data, shown by the solid lines, give individual determinations of k_6(IO + IO): (a) Kinetic measurement while monitoring IO concentration at the (2, 0) bandhead; (b) Kinetic measurement while monitoring IO concentration at the (1, 0) band.

In separate experiments we used a 0.25 m monochromator to measure the absorption cross-sections of NO_2 at 445.04 and 455.17 nm and found $\sigma_{445}^{\text{NO}_2} = 5.5 \times 10^{-19}$ cm^2 and $\sigma_{455}^{\text{NO}_2} = 4.4 \times 10^{-19}$ cm^2, respectively. At both wavelengths the spectrum of NO_2 is a continuum and $\sigma_\lambda = \sigma_\lambda^{\text{eff}}$. In the following, these cross-sections are used to account for NO_2 production in our data analysis model. The relevant cross-sections of I_2 are about $\sigma_{445}^{\text{I}_2} \approx 3 \times 10^{-20}$ cm^2 and $\sigma_{455}^{\text{I}_2} \approx 4 \times 10^{-20}$ cm^2 , which are sufficiently small that we can ignore the contributions to total absorbance by I_2.[47]

3.2. Determination of k_5(O + CF_3I) and k_6(IO + IO). Determinations of the rate coefficients k_5(O + CF_3I) and k_6(IO + IO) were made under a variety of pressure and gas-composition conditions (Table 1), both to check for pressure dependence of the rate coefficients and to assess the likelihood of aerosol formation within the reactor. Data sets were recorded in argon buffer (with no added NO) at total pressures of 1290 Pa (9.7 Torr) and 4000 Pa (31.2 Torr). Since the reaction rate coefficients obtained at both pressures were statistically the same, we report their averages.

Figure 3 shows representative absorbance data and the fit of these data that extracts one individual rate for k_5(O + CF_3I)

TABLE 1: Summary of the Experimental Conditions and Derived Rate Coefficients Obtained at 295 K for the O + CF_3I Reaction System

transition[a]	total press., Pa	partial press N_2O, Pa	partial press CF_3I, Pa	partial press NO, Pa	derived k_5,[b] cm^3 $molec^{-1}$ s^{-1}	derived k_6,[b] cm^3 $molec^{-1}$ s^{-1}	derived k_7,[b] cm^3 $molec^{-1}$ s^{-1}
IO (2, 0)	1252	34.4	4.9		$(6.0 \pm 0.4) \times 10^{-12}$		
IO (2, 0)	1290	34.4	4.9			$(10.7 \pm 0.8) \times 10^{-11}$	
IO (2, 0)	1302	34.1	4.8		$(6.0 \pm 0.8) \times 10^{-12}$	$(11.3 \pm 0.5) \times 10^{-11}$	
IO (2, 0)	1264	34.6	9.8		$(4.5 \pm 1) \times 10^{-12}$	$(12.0 \pm 0.7) \times 10^{-11}$	
IO (2, 0)	4010	83.4	11.7		$(6.2 \pm 0.4) \times 10^{-12}$	$(8.2 \pm 0.2) \times 10^{-11}$	
IO (2, 0)	4015	83.5	11.8		$(6.4 \pm 0.5) \times 10^{-12}$	$(8.3 \pm 0.2) \times 10^{-11}$	
IO (2, 0)	4015	83.5	11.9			$(9.8 \pm 0.4) \times 10^{-11}$	
IO (1, 0)	4015	83.5	11.9			$(8.8 \pm 0.8) \times 10^{-11}$	
IO (2, 0)	1241	34.1	4.8	0.13			$(2.4 \pm 0.1) \times 10^{-11}$
IO (2, 0)	1264	34.6	9.8	0.14			$(1.87 \pm 0.08) \times 10^{-11}$
IO (2, 0)	4010	83.4	11.7	0.16			$(1.48 \pm 0.06) \times 10^{-11}$
IO (2, 0)	1241	34.1	4.8	0.20			$(2.2 \pm 0.1) \times 10^{-11}$
IO (2, 0)	1264	34.6	9.8	0.20			$(1.78 \pm 0.08) \times 10^{-11}$
IO (2, 0)	4014	83.5	11.8	0.24			$(1.75 \pm 0.08) \times 10^{-11}$
IO (2, 0)	1241	34.1	4.8	0.27			$(2.21 \pm 0.1) \times 10^{-11}$
IO (2, 0)	1241	34.1	4.8	0.27			$(2.21 \pm 0.09) \times 10^{-11}$
IO (2, 0)	1264	34.6	9.8	0.27			$(1.74 \pm 0.08) \times 10^{-11}$
IO (2, 0)	4016	83.5	11.8	0.31			$(1.71 \pm 0.07) \times 10^{-11}$
IO (2, 0)	1241	34.1	4.8	0.33			$(2.27 \pm 0.09) \times 10^{-11}$
IO (2, 0)	1264	34.6	9.8	0.34			$(1.73 \pm 0.08) \times 10^{-11}$
IO (2, 0)	4016	83.5	11.8	0.39			$(1.92 \pm 0.07) \times 10^{-11}$
IO (2, 0)	1264	34.6	9.8	0.41			$(1.73 \pm 0.07) \times 10^{-11}$
IO (2, 0)	1264	34.6	9.8	0.47			$(1.7 \pm 0.2) \times 10^{-11}$
IO (1, 0)	4014	83.5	11.8	0.08			$(1.9 \pm 0.3) \times 10^{-11}$
IO (1, 0)	4016	83.5	11.8	0.16			$(1.3 \pm 0.2) \times 10^{-11}$
IO (1, 0)	4016	83.5	11.8	0.24			$(1.8 \pm 0.3) \times 10^{-11}$
IO (1, 0)	4019	83.6	11.8	0.31			$(1.5 \pm 0.2) \times 10^{-11}$
IO (1, 0)	4022	83.6	11.8	0.39			$(2.0 \pm 0.2) \times 10^{-11}$
IO (1, 0)	4020	83.6	11.8	0.47			$(2.1 \pm 0.2) \times 10^{-11}$

[a] IO (1, 0) denotes measurements at $\lambda_{CRDS} = 455.17$ nm and IO (2, 0) denotes measurements at $\lambda_{CRDS} = 445.04$ nm. [b] Rate coefficient lists the expanded uncertainty (2σ) of the precision.

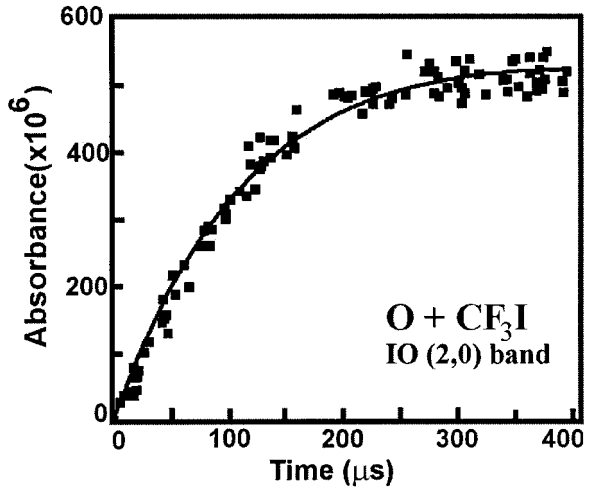

Figure 3. Kinetic measurement that determines $k_5(O + CF_3I)$. The squares show absorbance at 445.04 nm as a function of the time delay between the photolysis laser pulse that initiates the IO production process (reactions 1, 2, and 5) and the CRDS laser pulse that probes absorbance by IO radicals. The fit to the data, shown by the solid line, gives one determination of $k_5(O + CF_3I)$. The pressure in the experiment is 1252 Pa.

while monitoring the transient absorbance at the IO (2,0) bandhead at $\lambda_{CRDS} = 445.04$ nm. The average of all determinations from individual experiments yielded $k_5(O + CF_3I) = (5.8 \pm 1.5) \times 10^{-12}$ cm^3 $molec^{-1}$ s^{-1} (Table 2), where the uncertainty denotes two standard deviations. The model used to fit these data comprised reactions 5 and 6. According to the model, the photolysis event dissociates between 0.01 and 0.05% of the irradiated N_2O to yield maximum IO concentrations ranging between 1.0×10^{12} radicals cm^{-3} and 1.2×10^{13} radicals cm^{-3}. Under all of the conditions employed, the model predicts that IO formation was >95% complete within 500 μs.

In a previous study, CRDS was used to detect rotational lines of the IF B $^3\Pi$ $(0^+)-X$ $^1\Sigma^+(0^+)$ transition with good sensitivity.[45] Since the spectrum of IF overlaps the IO (2, 0) and IO (1, 0) bands and is readily observed by CRDS, the absence of any IF signal indicates that the production of IF by reaction 5b is insignificant.

Figure 2 shows representative absorbance data obtained while measuring IO concentrations with the IO (2, 0) and IO (1, 0) bands. The solid lines are the fits that obtain individual measurements of $k_6(IO + IO)$. The fits were also computed with a numerical model comprising of reactions 5 and 6. The average of data (Table 1) obtained by monitoring the IO (2, 0) bandhead yielded $k_6(IO + IO) = (1.0 \pm 0.3) \times 10^{-10}$ cm^3 $molec^{-1}$ s^{-1} (Table 2). Averages of data measured at 1250 and 4000 Pa were identical. When monitoring IO radicals with the (1, 0) band, we obtained $k_6(IO + IO) = (8.8 \pm 1.2) \times 10^{-11}$ cm^3 $molec^{-1}$ s^{-1}, where this determination of $k_6(IO + IO)$ is based on our determination of σ_{455}^{IO}. The stated uncertainty of each determination of $k_6(IO + IO)$ denotes two standard deviations and contains the uncertainty in the absorption cross-section.

When computing fits of the kinetic data, adding reaction 8 to the model had little effect and produced essentially the same reaction rate coefficient. The insensitivity of the model to reaction 8 occurs because the concentrations of $O(^3P)$ and IO are small relative to that of CF_3I. We also attempted to fit the IO radical decay data using models that explicitly accounted for the quenching of $O(^1D)$ via reaction 2 and for NO produced by reaction 3a. Presumably, this more extensive model would account for any enhanced loss of IO from a cross-reaction with NO (reaction 7), where the NO is generated by reaction 3a.

TABLE 2: Summary of the Methods, Conditions, and Rate Coefficients at 295 K of this Work and Previous Studies of the Primary Reactions in the O + CF_3I Reaction System. Rate Coefficients are Listed for Temperatures of 298 K unless Otherwise Indicated[a]

298 K rate coefficient,[a] cm^3 $molec^{-1}$ s^{-1}	pressure, Pa	technique[b] (species detected)	ref	comments
				k_5 ($O(^3P)$ + CF_3I)
$(5.8 \pm 1.5) \times 10^{-12}$	1250, 4000	CRDS (IO)	this work	T = 295 K.
$(1.1 \pm 0.3) \times 10^{-11}$ [c]	800	RF (O^3P)	57	
$(5.3 \pm 0.08) \times 10^{-12}$	6700	LIF (IO)	10	Temperature dependence over range 230 to 310 K and a rate expression are reported.
$(4.3 \pm 0.2) \times 10^{-12}$	13300	RF (O^3P)	41	Branching ratio, temperature dependence over the range 213 to 364 K and a rate expression for k_5 are reported.
		LIF (IO)		
$(6.5 \pm 1.5) \times 10^{-12}$ [c]	1330	LIF (IF)	58	IF was a product of complex chemistry and not from reaction 5.
				k_6 (IO + IO)
$(1.0 \pm 0.3) \times 10^{-10}$	1250, 4000	CRDS (IO)	this work	T = 295 K.
$(9.9 \pm 3.0) \times 10^{-11}$	53200	UVA (IO)	8	T = 250 to 320 K.
$(8.0 \pm 1.8) \times 10^{-11}$	7980−79800	UVA (IO)	7	T = 295 K
$(6.6 \pm 2) \times 10^{-11}$ [c]	101080	UVA (IO)	9	T = 300 K.
$(5.6 \pm 1.2) \times 10^{-11}$	270−93100	UVA (IO)	42	T = 250 to 373 K.
4×10^{-10}	101080	UVA (IO)	44	T = 303 K. See text.
$(5.5 \pm 0.8) \times 10^{-11}$	240−670	MS (IO)	59	
$(3.0 \pm 1.1) \times 10^{-11}$ [c]	133	MS (IO)	60	
				k_7 (IO + NO)
$(1.9 \pm 0.5) \times 10^{-11}$	1250, 4000	CRDS (IO)	this work	T = 295 K.
$(2.17 \pm 0.22) \times 10^{-11}$	5330−26700	UVA (IO)	16	Temperature dependence over the range 242 to 359 K and a rate expression are reported. Here k_6 is independent of pressure.
$(1.9 \pm 0.1) \times 10^{-11}$	670−13330	LIF (IO)	15	Temperature dependence over the range 237 to 346 K and a rate expression are reported.
$(2.8 \pm 0.2) \times 10^{-11}$	53−106	LIF (IO)	13	
$(1.67 \pm 0.16) \times 10^{-11}$	270	MS (IO)	61	

[a] Uncertainties denote two standard deviations. [b] CRD = cavity ring-down, RF = resonance fluorescence, LIF = laser induced fluorescence, UVA = UV-visible absorption, MS = mass spectrometry. [c] Uncertainty not explained but is presumed to be two standard deviations.

According to this reaction scheme, NO production will vary as functions of Ar, CF_3I, and N_2O densities within the reactor. However, neither k_5(O + CF_3I) nor k_6(IO + IO) exhibited statistically meaningful dependencies as total pressure of argon buffer changed from 1250 to 4000 Pa, as CF_3I density was varied by a factor of 3, and as N_2O density was varied by a factor of 10. Since no effect was observed in the data, we discarded reactions 2, 3a, and 7 from the final model.

Previously, Laszlo et al.[7] noted that increased CF_3I concentration also increased the propensity for aerosol formation. Aerosols were observed to increase the apparent rate of k_6(IO + IO). During the present work k_6(IO + IO) did not vary as a function of initial CF_3I concentration. This invariance is additional evidence that aerosol formation was minimal or absent during our kinetics determinations.

In our model the decay of IO is presumed to occur only through reaction 6; however, we can also consider the effects of CF_3 and of I atoms upon the determination of k_6(IO + IO). Reaction rate coefficients of CF_3 with itself, with $O(^3P)$,[48,49] with I atoms,[50] and with CF_3I [51] are known. These reactions are slow, and significant concentrations of CF_3 persist. Presumably the reaction

$$CF_3 + IO \rightarrow CF_3O + I \qquad \Delta_rH^o_{298.15} = -206 \text{ kJ mol}^{-1}\ ^{52-54} \quad (11a)$$

$$\rightarrow CF_2O + IF \qquad \Delta_rH^o_{298.15} = -388 \text{ kJ mol}^{-1} \quad (11b)$$

might perturb rate coefficient determinations. Adding the known rate coefficients to the model and refitting the data to find k_{11}(CF_3 + IO) degrades the quality of the fits for k_5(O + CF_3I) and k_6(IO + IO) and increases the accumulated error. No experimental data support the activity of reaction 11. Since we do not observe IF absorption bands overlapping the IO (2, 0) and IO (1, 0) bands, we conclude that reaction 11b played no role under the conditions of our kinetic studies. Gilles et al.[41] attempted to observe CF_3O during their study without success. Although their search was directed toward characterizing reaction 5, this negative result suggests that reaction 11a is comparatively slow. We conclude that CF_3 radicals are unlikely to have perturbed the temporal evolution of IO during the present experiments.

Evaluating the effects of I atoms upon determinations of k_6(IO + IO) is complicated by our incomplete knowledge of reaction 6. By monitoring I_2 absorption, Harwood et al.[8] determined that all I atoms and IO radicals eventually revert to I_2. The growth of I_2 absorption followed second order kinetics with relatively slow rate constants ranging between 3×10^{-13} cm^3 $molec^{-1}$ s^{-1} and 1.2×10^{-12} cm^3 $molec^{-1}$ s^{-1}. Laszlo et al.[7] observed similar I_2 signals and noted their pressure dependence. To account for these observations, Harwood et al.[8] proposed the reaction scheme

$$IO + I\ (+M) \rightarrow I_2O \quad (12)$$

$$I + I_2O \rightarrow I_2 + IO \quad (13)$$

The formation of I_2 through reactions 12 and 13 shows a second-order behavior because the IO production reaction

$$O(^3P) + I_2 \rightarrow IO + I \quad (14)$$

creates equal concentrations of IO and I atoms.

Because the present study monitors IO radicals, reactions 12 and 13 will tend to form a null cycle with little net effect on the absorption trace. Furthermore, during this study the importance of reactions 12 and 13 is greatly diminished, owing to the absence of I atoms at early times. Using the absorption cross-sections of CF_3I [55] and N_2O [36] at 193 nm, we estimate that the initial molar concentration of I atoms is < 2.5% of the initial

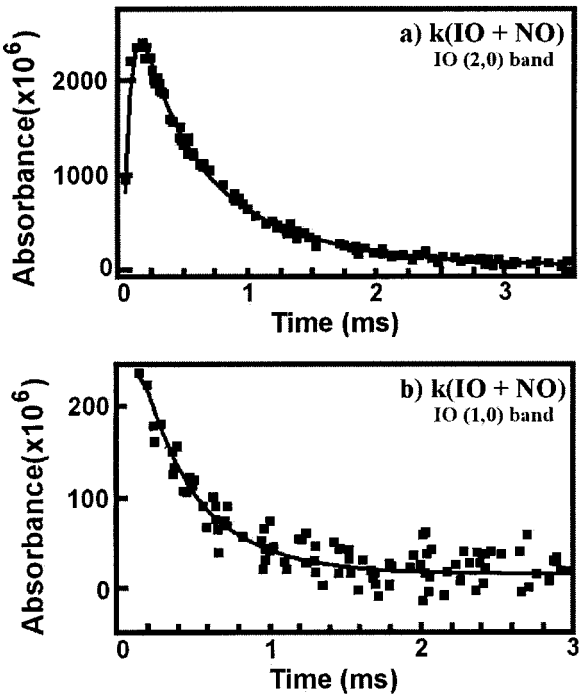

Figure 4. Kinetic measurements that determine k_7(IO + NO). The squares show absorbance as a function of the time delay between the photolysis laser pulse that initiates IO formation and the CRDS laser pulse that probes absorbance by the IO radical and NO_2. The fits of the data, shown by the solid lines, give individual determinations of k_7(IO + NO): (a) Kinetic measurement while monitoring IO concentration at the (2, 0) bandhead. The NO density is 6.77×10^{13} molec cm^{-3}; (b) Kinetic measurement while monitoring IO concentration at the (1, 0) band. The NO density is 1.13×10^{14} molec cm^{-3}.

$O(^3P)$ atoms. Our source of IO radicals (reaction 5) does not produce I atoms. Reactions 6b and 6d provide a comparatively meager source of I atoms. Thus, the I atoms in our present study are expected to have little effect on the observed rate coefficients.

3.3. Determination of k_7(IO + NO). Kinetics measurements of reaction 7, IO + NO, were undertaken at a total pressure in the reaction cell of near 1250 Pa (9.4 Torr) and 4000 Pa (30.1 Torr) (Table 1). At pressures of ~1250 Pa, typical flow rates of the constituent gases were 750 sccm Ar, 30 sccm N_2O, and 3 sccm CF_3I, and neat NO was added at flow rates varying from 0.1 to 0.25 sccm. At pressures near 4000 Pa typical flow rates were 1000 sccm Ar, 30 sccm N_2O, and 3 sccm CF_3I, and a mixture of 4.80% NO in argon was added with flow rates from 0.5 to 3.0 sccm. The system absorbance was monitored either at the IO (2, 0) bandhead at 445.04 nm or with the IO (1, 0) band at 455.17 nm. Detection of IO at the bandhead of the A−X (1, 0) band gave poorer quality data sets because the absorption via this band is weaker than via the A−X (2, 0) band. Also, the effects of NO_2 absorption at longer times are more pronounced since the ratio of the IO/NO_2 absorption cross-sections is closer to unity.

Figure 4 shows the absorbance data and the fit that obtains individual measurements of k_7(IO + NO). Kinetic traces obtained while monitoring the IO (2, 0) and IO (1, 0) bands are shown. Each data set exhibited a linear pseudo-first-order plot of k_{obs} as a function of NO concentration; however, to compensate for side reactions, we computationally fit the data directly using a kinetic model comprising of reactions 5, 6, and 7. Since added NO rapidly depletes CF_3 radicals[56] and I atoms[36] via the termolecular reactions these radicals do not affect

$$CF_3 + NO\ (+M) \rightarrow CF_3NO \quad (15)$$

$$I + NO\ (+M) \rightarrow INO \quad (16)$$

determinations of k_7(IO + NO). For these simulations we have used the k_5 and k_6 of this work (Table 2). Reaction 7 generates NO_2 that has an increasing absorbance contribution at λ_{CRDS}. Consequently, the numerical model incorporates the appropriate optical absorption coefficients and simulates the combined absorbance by IO and NO_2. The average of all individual kinetic traces obtained while monitoring the IO (2, 0) bandhead is k_7(IO + NO) = $(1.9 \pm 0.5) \times 10^{-11}$ cm^3 molec^{-1} s^{-1}. The average of all kinetic traces obtained while monitoring the IO (1, 0) band is k_7(IO + NO) = $(1.8 \pm 0.6) \times 10^{-11}$ cm^3 molec^{-1} s^{-1}. Since the relative cross-sections of IO and NO_2 differ for the IO (2, 0) and IO (1, 0) bands, the good agreement of k_7(IO + NO) derived at each wavelength is a measure of consistency of the overall model.

4. Discussion

Table 2 summarizes the ambient temperature (295 K) rate coefficients determined during this study of the reaction system $O(^3P) + CF_3I$. Table 2 also lists the results reported by previous studies; first, by detection method for IO, and then, by chronology. Except as noted, these ambient temperature rate coefficients are for 298 K. Uncertainties listed with each rate coefficient denote two standard deviations and propagate the uncertainty in the absorption cross-sections. Previous determinations of k_6(IO + IO) and k_7(IO + NO) have used different sources for $O(^3P)$, different iodine atom donors, pressure ranges, and detection techniques. As seen in Table 2, the present rate coefficients derived from CRDS measurements are in excellent agreement with the more current determinations and add to consensus among these rate coefficients. The only serious disagreement is with the rate coefficient of Inoue et al.[13] for k_7(IO + NO). Cox and Coker[44] indicated that their anomalously high k_6(IO + IO) (Table 2) contains contributions from termolecular and heterogeneous processes. Our measurements of k_7(IO + NO) at 1200 and 4000 Pa total pressure show no significant variation with pressure, thereby supporting the data of Daykin and Wine[16] over the pressure range 5330 and 26700 Pa (40 and 200 Torr) and of Turnipseed et al.[15] over the pressure range 670 and 13330 Pa (5 and 100 Torr). These accumulated data indicate that k_7(IO + NO) is independent of pressure for pressures above 1330 Pa (10 Torr). Our rate coefficients also show no dependence on the concentration of CF_3I, which provides additional evidence that aerosol formation in the reactor can be discounted under our experimental conditions.

To date, the validation of CRDS for determination of rate coefficients has been sparse and hence the current investigation constitutes a contribution to the evidence supporting the use of this recently developed spectroscopic technique for such studies. Moreover, this study provides validation that CRDS can accurately determine rate coefficients for reactions studied in first order (k_5 and k_7) and in second order (k_6).

This study also provides practical data regarding the range of absorption coefficients that are of use for kinetics measurements with CRDS. Using the IO (2, 0) band and assuming a minimum measurable absorbance of 10^{-7} cm^{-1}, we estimate that the detection limit for IO radicals is 1.4×10^9 molec cm^{-3}. By obtaining readily available mirrors of higher reflectivity this limit could be improved by another factor of 10. However, the more interesting aspect is that measurements can be obtained

under less than ideal conditions. At $\sigma_{455}^{IO} = 7.3 \times 10^{-18}$ cm^2, the IO (1, 0) absorption cross-section is an order of magnitude smaller than the IO (2, 0) bandhead. Furthermore, measurements using the IO (1, 0) band suffer greater interference from an increasing population of absorbing NO_2 than when using than IO (2, 0) band. Despite these hindrances, we were able to follow the decay of IO for about three 1/e lifetimes using the IO (1, 0) band for peak radical densities of $\sim 5 \times 10^{12}$ cm^{-3}. Importantly, agreement is found for the determinations of k_6 and k_7 at both wavelengths. As expected, rate coefficients determined using the IO (1, 0) band have larger uncertainties and any study using such small cross-sections can examine only a restricted range of experimental conditions. Even so, good rate coefficients can be obtained.

Acknowledgment. The visit of A.J.O.E. to NIST was made possible by the award of a NATO travel grant (Ref. CRG 950105). A.J.O.E. thanks the Royal Society for the award of the Eliz. Challenor Research Fellowship. We thank Drs. R. E. Huie, B. Laszlo, and A. Fahr for experimental assistance in the course of this study and Dr. Michael Kurylo for helpful comments and suggestions during the preparation and revision of this manuscript.

References and Notes

(1) Wayne, R. P.; Poulet, G.; Biggs, P.; Burrows, J. P.; Cox, R. A.; Crutzen, P. J.; Hayman, G. D.; Jenkin, M. E.; Le Bras, G.; Moortgat, G. K.; Platt, U.; Schindler, R. N. *Halogen oxides: radicals, sources and reservoirs in the laboratory and in the atmosphere*, Air Pollution Research Report 55, Directorate-General Science, Research and Development Environment research programme, European Commission, 1995.

(2) Davis, D.; Crawford, J.; Liu, S.; McKeen, S.; Bandy, A.; Thornton, D.; Rowland, F.; Blake, D. *J. Geophys. Res.* **1996**, *101*, 2135.

(3) Solomon, S.; Garcia, R. R.; Ravishankara, A. R. *J. Geophys. Res.* **1994**, *99*, 20491.

(4) Sturges, W. T.; Barrie, L. A. *Atmos. Environ.* **1988**, *22*, 1179.

(5) Alicke, B.; Hebestreit, K.; Platt, U.; Carpenter, L. J.; Sturges, W. *Ann. Geophys.* **1998**, *16* (Suppl. II), C716.

(6) Laszlo, B.; Kurylo, M. J.; Huie, R. E. *J. Geophys. Res.* **1997**, *102*, 1523.

(7) Laszlo, B.; Kurylo, M. J.; Huie, R. E. *J. Phys. Chem.* **1995**, *99*, 11701.

(8) Harwood, M. H.; Burkholder, J. B.; Hunter, M.; Fox, R. W.; Ravishankara, A. R. *J. Phys. Chem. A* **1997**, *101*, 853.

(9) Stickel, R. E.; Hynes, A. J.; Bradshaw, J. D.; Chameides, W. L.; Davis, D. D. *J. Phys. Chem.* **1988**, *92*, 1862.

(10) Hölscher, D.; Fockenberg, C.; Zellner, R. *Berichte Der Bunsen-Ges. Phys. Chem.* **1998**, *102*, 716.

(11) Gilles, M. K.; Turnipseed, A. A.; Burkholder, J. B.; Ravishankara, A. R. *Chem. Phys. Lett.* **1997**, *272*, 75.

(12) Gilles, M. K.; Turnipseed, A. A.; Burkholder, J. B.; Ravishankara, A. R.; Solomon, S. *J. Phys. Chem. A*, **1997**, *101*, 5526.

(13) Inoue, G.; Suzuki, M.; Washida, N. *J. Chem. Phys.* **1983**, *79*, 4730.

(14) Turnipseed, A. A.; Gilles, M. K.; Burkholder, J. B.; Ravishankara, A. R. *J. Phys. Chem.* **1997**, *101*, 5517.

(15) Turnipseed, A. A.; Gilles, M. K.; Burkholder, J. B.; Ravishankara, A. R. *Chem. Phys. Lett.* **1995**, *242*, 427.

(16) Daykin, E. P.; Wine, P. H. *J. Phys. Chem.* **1990**, *94*, 4528.

(17) Buben, S. N.; Larin, I. K.; Trofimova, E. M. *Kinet. Catal.* **1995**, *36*, 745.

(18) Daykin, E. P.; Wine, P. H. *J. Geophys. Res.* **1990**, *95*, 18547.

(19) O'Keefe, A.; Deacon, A. G. *Rev. Sci. Instrumen.* **1988**, *59*, 2544.

(20) Scherer, J. J.; Paul, J. B.; O'Keefe, A.; Saykally, R. J. *Chem. Rev.* **1997**, *97*, 25.

(21) Wheeler, M. D.; Newman, S. M.; Orr-Ewing, A. J.; Ashfold, M. N. R. *J. Chem. Soc. Faraday Trans.* **1998**, *94*, 337.

(22) Yu, T.; Lin, M. C. *Int. J. Chem. Kinet.* **1993**, *25*, 875.

(23) Yu, T.; Lin, M. C. *J. Am. Chem. Soc.* **1994**, *116*, 9571.

(24) Yu, T.; Lin, M. C. *J. Phys. Chem.* **1995**, *99*, 8599.

(25) Yu, T.; Lin, M. C. *Int. J. Chem. Kinet.* **1994**, *26*, 771.

(26) Yu, T.; Lin, M. C. *J. Phys. Chem.* **1994**, *98*, 9697.

(27) Diau, E. W.; Yu, T.; Wagner, M. A. G.; Lin, M. C. *J. Phys. Chem.* **1994**, *98*, 4034.

(28) Atkinson, D. B.; Hudgens, J. W *J. Phys. Chem. A*, **1999**, *103*, 4242.

(29) Atkinson, D. B.; Hudgens, J. W. *J. Phys. Chem. A* **1997**, *101*, 3901.

(30) Zhu, L.; Johnston, G. *J. Phys. Chem.* **1995**, *99*, 15114.

(31) Atkinson, D. B.; Hudgens, J. W. *J. Phys. Chem. A*, submitted.

(32) Atkinson, D. B.; Hudgens, J. W., in preparation.

(33) Wheeler, M. D.; Newman, S. M.; Ishiwata, T.; Kawasaki, M.; Orr-Ewing, A. J. *Chem. Phys. Lett.* **1998**, *285*, 346.

(34) *Nonlinear Levenberg−Marquardt fitting virtual instrument*, Labview 4.0, National Instruments Corporation, Austin, TX, 1994−1995.

(35) Braun, W. *Int. J. Chem. Kinet.* **1988**, *20*, 51.

(36) DeMore, W. B.; Sander, S. P.; Golden, D. M.; Hampson, R. F.; Kurylo, M. J.; Howard, C. J.; Ravishankara, A. R.; Kolb, C. E.; Molina, M. J. *Chemical kinetics and photochemical data for use in stratospheric modeling. Evaluation number 12*, JPL publication 97-4, 1997.

(37) Davidson, J. A.; Schiff, H. I.; Brown, T. J.; Streit, G. E.; Howard, C. J. *J. Chem. Phys.* **1978**, *69*, 1213.

(38) Doroshenko, V. M.; Kudryavtsev, N. N.; Smetanin, V. V. *High Energy Chem.* **1992**, *26*, 227.

(39) Takahashi, K.; Wada, R.; Matsumi, Y.; Kawasaki, M. *J. Phys. Chem.* **1996**, *100*, 10145.

(40) Thompson, J. E.; Ravishankara, A. R. *Int. J. Chem. Kinet.* **1993**, *25*, 479.

(41) Gilles, M. K.; Turnipseed, A. A.; Talukdar, R. K.; Rudich, Y.; Villalta, P. W.; Huey, L. G.; Burkholder, J. B.; Ravishankara, A. R. *J. Phys. Chem.* **1996**, *100*, 14005.

(42) Sander, S. P. *J. Phys. Chem.* **1986**, *90*, 2194.

(43) Himmelmann, S.; Orphal, J.; Bovensmann, H.; Richter, A.; Ladstätter-Weissenmayer, A.; Burrows, J. P. *Chem. Phys. Lett.* **1996**, *251*, 330.

(44) Cox, R. A.; Coker, G. B. *J. Phys. Chem.* **1983**, *87*, 4478.

(45) Newman, S. M.; Howie, W.; Lane, I. C.; Upson, M.; Orr-Ewing, A. J. *J. Chem. Soc., Faraday Trans.* **1998**, *94*, 2681.

(46) Zalicki, P.; Zare, R. N. *J. Chem. Phys.* **1995**, *102*, 2708.

(47) Calvert, J. G.; Pitts, J. N. *Photochemistry*; Wiley: New York, 1966.

(48) Ryan, K. R.; Plumb, I. C. *J. Phys. Chem.* **1982**, *86*, 4678.

(49) Tsai, C.; Belanger, S. M.; Kim, J. T.; Lord, J. R.; McFadden, D. L. *J. Phys. Chem.* **1989**, *93*, 1916.

(50) Skorobogatov, G. A.; Seleznev, V. G.; Slesar, O. N. *Dokl. Phys. Chem. (Engl. Transl.)* **1976**, *231*, 1292.

(51) Andreeva, T. L.; Kuznetsova, S. V.; Maslov, A. I.; Sobel'man, I. I.; Sorokin, V.N. *High Energy Chem.* **1972**, *6*, 368.

(52) Zachariah, M.; Westmoreland, P.; Burgess, D. R.; Tsang, W. *J. Phys. Chem.* **1996**, *100*, 9737.

(53) Chase, M. W., Jr. *J. Phys. Chem. Ref. Data* **1996**, *25*, 1297.

(54) Chase, M. W., Jr. *J. Phys. Chem. Ref. Data, Monograph 9*, **1998**.

(55) Fahr, A.; Nayak, A. K.; Huie, R. E. *Chem. Phys.* **1995**, *199*, 275.

(56) Ley, L.; Masanet, J.; Caralp, F.; Lesclaux, R. *J. Phys. Chem.* **1995**, *99*, 1953.

(57) Addison, M. C.; Donovan, R. J.; Garraway, J. *Chem. Soc. Faraday Discuss.* **1979**, *67*, 286.

(58) Watson, T. A.; Addison, M.; Wittig, C. *Chem. Phys.* **1983**, *78*, 57.

(59) Barnes, I.; Bastian, V.; Becker, K. H.; Overath, R. D. *Int. J. Chem. Kinet.* **1991**, *23*, 579.

(60) Martin, D.; Jourdain, J. L.; Laverdet, G.; Le Bras, G. *Int. J. Chem. Kinet.* **1987**, *19*, 503.

(61) Ray, G. W.; Watson, R. T. *J. Phys. Chem.* **1981**, *85*, 2955.